The interaction of organic adsorbate vibrations with substrate lattice waves in methyl-Si(111)-(1×1)

Ryan D. Brown, Zachary M. Hund, Davide Campi, Leslie E. O'Leary, Nathan S. Lewis, M. Bernasconi, G. Benedek, and S. J. Sibener

Citation: The Journal of Chemical Physics **141**, 024702 (2014); doi: 10.1063/1.4886810
View online: http://dx.doi.org/10.1063/1.4886810
View Table of Contents: http://scitation.aip.org/content/aip/journal/jcp/141/2?ver=pdfcov
Published by the AIP Publishing

The interaction of organic adsorbate vibrations with substrate lattice waves in methyl-Si(111)-(1 × 1)

Ryan D. Brown,[1] Zachary M. Hund,[1] Davide Campi,[2] Leslie E. O'Leary,[3] Nathan S. Lewis,[3] M. Bernasconi,[2] G. Benedek,[2,4] and S. J. Sibener[1,a)]

[1]*The James Franck Institute and Department of Chemistry, The University of Chicago, 929 E. 57th Street, Chicago, Illinois 60637, USA*
[2]*Dipartimento di Scienza dei Materiali, Universitá di Milano-Bicocca, Via Cozzi 53, 20125 Milano, Italy*
[3]*Beckman Institute and Kavli Nanoscience Institute, Division of Chemistry and Chemical Engineering, 210 Noyes Laboratory, 127-72, California Institute of Technology, Pasadena, California 91125, USA*
[4]*Donostia International Physics Center (DIPC), Universidad del País Vasco (EHU), 20018 Donostia / San Sebastian, Spain*

(Received 1 May 2014; accepted 23 June 2014; published online 9 July 2014)

A combined helium atom scattering and density functional perturbation theory study has been performed to elucidate the surface phonon dispersion relations for both the CH_3-Si(111)-(1 × 1) and CD_3-Si(111)-(1 × 1) surfaces. The combination of experimental and theoretical methods has allowed characterization of the interactions between the low energy vibrations of the adsorbate and the lattice waves of the underlying substrate, as well as characterization of the interactions between neighboring methyl groups, across the entire wavevector resolved vibrational energy spectrum of each system. The Rayleigh wave was found to hybridize with the surface rocking libration near the surface Brillouin zone edge at both the $\bar{M}$-point and $\bar{K}$-point. The calculations indicated that the range of possible energies for the potential barrier to the methyl rotation about the Si-C axis is sufficient to prevent the free rotation of the methyl groups at a room temperature interface. The density functional perturbation theory calculations revealed several other surface phonons that experienced mode-splitting arising from the mutual interaction of adjacent methyl groups. The theory identified a Lucas pair that exists just below the silicon optical bands. For both the CH_3- and CD_3-terminated Si(111) surfaces, the deformations of the methyl groups were examined and compared to previous experimental and theoretical work on the nature of the surface vibrations. The calculations indicated a splitting of the asymmetric deformation of the methyl group near the zone edges due to steric interactions of adjacent methyl groups. The observed shifts in vibrational energies of the -CD_3 groups were consistent with the expected effect of isotopic substitution in this system. © *2014 AIP Publishing LLC*. [http://dx.doi.org/10.1063/1.4886810]

I. INTRODUCTION

The functionalization of crystalline silicon surfaces by organic adlayers[1–3] has potential applications ranging from passivation and functionalization of silicon nanowires,[4,5] the passivation and functionalization of photoelectrodes in electrochemical cells,[6–8] and the fabrication of biological sensors.[9,10] Si(111) surfaces can be terminated with methyl groups in a highly controlled manner, which results in coverage by a full monolayer[6] with essentially every Si atom on the surface bonded to a methyl group. Relative to the hydrogen-terminated Si(111) surface, methyl-terminated Si(111) surfaces exhibit enhanced resistance to oxidation in air.[11,12] The vibrational features of methyl-terminated silicon surfaces impact the thermal properties and the ability of the surface to accommodate energy, so these vibrational properties have recently been studied both experimentally[13–19] and theoretically.[17,20] A comprehensive analysis of the surface-phonon dispersion relations along the entire surface Brillouin zone (SBZ), as well as the effect of isotopic loading on vibrations, which has been extensively studied for the hydrogen-terminated silicon(111) interface,[21–23] is, therefore, important to advance the understanding of the CH_3-Si(111) system.

In the present work we report a combined experimental and theoretical study of surface phonons for both CH_3-Si(111)-(1 × 1) and CD_3-Si(111)-(1 × 1) by means of helium atom scattering (HAS) measurements and *ab initio* density functional perturbation theory (DFPT) calculations. The combination of experimental HAS measurements and DFPT-based theoretical analysis of the surface phonons and molecular vibrations provides insight into the interplay of the vibrations of interfacial methyl group with those of the silicon lattice. In particular, the interaction of surface molecular librations with the Rayleigh wave (RW), a low-energy surface acoustic phonon, for both the CH_3- and CD_3-terminated surfaces has been evaluated. Additionally, the barrier to the rotation of the methyl groups about the Si-C axis has been elucidated, and the importance of that barrier to the surface structure was investigated in detail. The calculations have also provided a comprehensive description of surface phonon modes which have not yet been observed experimentally, either due

a)Author to whom correspondence should be addressed. Electronic mail: s-sibener@uchicago.edu

to experimental limitations of the method employed or due to physical limitations such as symmetry constraints or weak modulation of the surface charge density distribution.[24] The vibrational modes of the methyl group have also been evaluated, and the theoretical results have been compared with previous experimental and computational studies to facilitate evaluation of the impact of isotopic substitution on the vibrations of the terminal organic group.

II. EXPERIMENTAL AND COMPUTATIONAL DETAILS

A. Preparation of the CH_3-Si(111) and CD_3-Si(111) surfaces

The alkylation of hydrogen terminated Si(111) interfaces using a chlorination, alkylation scheme has been reported elsewhere.[25] The particular scheme employed to generate the interfaces used in this study is as follows. Water with an 18.2 MΩ resistivity (Barnstead Nanopure) was used throughout the preparation of the surfaces. The n-Si wafers (Virginia Semiconductor, oriented ±0.1° to the (111) plane, phosphorus doped to 1 Ω cm resistivity) were cut to size and cleaned by sequential rinsing in water, methanol, acetone, methanol, and then water. Wafer pieces were further cleaned and oxidized in a piranha solution (1:3 30% $H_2O_{2(aq)}$:concentrated $H_2SO_{4(aq)}$; Caution – piranha solution reacts violently with organic compounds) at 90 °C for 10 min, then rinsed with a copious amount of water, and were quickly dried under a stream of $N_{2(g)}$. These wafers were immediately etched for 18 s in buffered HF (Transene Co.), drained, promptly rinsed with water, and submerged in an $Ar_{(g)}$ purged 11 M $NH_4F_{(aq)}$ for 9 min to obtain an atomically flat H-terminated Si(111) surface. While submerged in the $NH_4F_{(aq)}$ solution, the samples were periodically agitated to prevent bubble formation on the surface. After etching, the samples were rinsed with water, dried under a $N_{2(g)}$ stream, and placed in a $N_{2(g)}$-purged flushbox, in which the concentration of $O_{2(g)}$ was < 10 ppm.

The H-terminated Si(111) wafers were then placed in a saturated solution of PCl_5 (99.998% Alfa Aesar) in anhydrous chlorobenzene (Aldrich) to which a few grains of benzoyl peroxide (a radical initiator) had been added. The solution was maintained at 90 °C for 45 min, and then was allowed to cool for 5–10 min. The flask was drained, and the wafer pieces were rinsed with chlorobenzene, then anhydrous tetrahydrofuran (THF) (Aldrich). The resulting chloride-terminated Si(111) wafers were submerged in a 1.0 M solution of CH_3-MgCl in THF (diluted from 3.0 M CH_3-MgCl, Sigma) and the reaction vessel was held at 50 °C–60 °C for at least 3 h to produce methyl-terminated Si(111) surfaces. After methylation, the wafer pieces were removed from solution and rinsed thoroughly with THF. The wafers were removed from the flushbox and sonicated sequentially in THF, methanol, and water for 10 min each, and then rinsed with water and dried under a stream of $N_{2(g)}$.

B. Helium atom scattering techniques

The surface phonon dispersion relations were obtained using an ultra-high vacuum (UHV) helium atom scattering (HAS) apparatus, which is described in detail elsewhere.[26] The apparatus consisted of three regions: a differentially pumped beam source, a UHV sample chamber, and a rotatable detector arm with a total flight path of 1.0778 m (chopper-to-crystal distance of 0.4996 m, crystal-to-ionizer distance of 0.5782 m). A nearly mono-energetic beam of atoms ($\Delta v/v \leq 1\%$, FWHM) was produced by the supersonic expansion of helium through a nozzle source, the center of which was captured by a conical skimmer and collimated by two apertures into a 4 mm spot at the sample. The temperature of the supersonic nozzle was controlled by heating against cooling which is provided by a closed-cycle helium refrigerator. The beam was mechanically modulated by a chopper wheel in the first differentially pumped region of the beam line for the purpose of making energy resolved measurements. The sample was mounted on a six axis manipulator in the UHV chamber (base pressure 3×10^{-10} torr) and the sample temperature was controlled by a button heater and a second closed-cycle helium refrigerator. The scattered atoms entered the rotatable detector arm, were ionized via electron bombardment, and then filtered using a quadrupole mass spectrometer. The detector arm has a 40° range of motion, and the overall instrumental resolution function was 0.45° FWHM. The geometry of this apparatus allows for a range of incident angles (θ_i) of roughly 20°–40° from the surface normal, with the accessible scattering angles (θ_f) being dependent on the detector arm range of motion. The beam energies employed in these experiments were 32–67 meV, and the surface temperatures used were generally from 140 to 200 K. At the start of each set of experiments, the sample was first flashed to 600 K to remove trace adsorbates from the surface, and then quenched to the sample temperature that was used during data acquisition. Prior to data collection at a given angle of incidence, He diffraction spectra were obtained to verify the crystallographic alignment of the sample. Time-of-flight spectra were obtained using single-slit chopping patterns (≈1% duty cycle) and generally consisted of 1×10^6 to 1.5×10^6 shots, corresponding to acquisition times of 20–30 min. When necessary, composite spectra were produced for enhanced signal-to-noise by the addition of consecutive spectra acquired under identical conditions, with a sample temperature flash to 350 K between runs to remove any surface adsorbates.

C. Density functional perturbation theory computational details

The dynamical properties of the CH_3-Si(111) and CD_3-Si(111) surfaces were calculated using density functional perturbation theory, as implemented in the QUANTUM-ESPRESSO package,[27] using ultrasofts pseudopotentials[28] and the Perdew-Burke-Ernzerhof (PBE) approximation for the exchange-correlation energy functional.[29] The electronic wavefunctions were expanded in plane waves up to a 28 Ry energy cutoff and a 280 Ry charge density cutoff. The surface was modelled using a slab geometry and periodic boundary conditions (PBC), with slabs composed of 12 silicon atom layers with methyl groups adsorbed on both sides, which were separated by a vacuum gap having a width of 12 Å. The SBZ was sampled over a Monkhorst-Pack grid of $6 \times 6 \times 1$ k-points.[30] Atomic positions were relaxed until the forces were

below a 5×10^{-5} a.u. threshold. The optimized structure calculated for both CH_3-Si(111) and CD_3-Si(111) had a C-H(D) bond length of 1.099 Å, a C-Si bond length of 1.918 Å, and a bulk Si-Si bond length of 2.352 Å. The distance between the first and second silicon layers was expanded by $\Delta d_{12} = 0.02$ Å, and the distance between the second and third silicon layers is expanded by $\Delta d_{23} = 0.01$ Å with respect to the ideal bulk-truncated positions. These lattice distortions are contrary to what was calculated for the H-Si(111)-(1 × 1) surface, where Δd_{12} and Δd_{23} are contracted by 0.03 Å and 0.01 Å, respectively, relative to the ideal bulk-truncated positions. The dihedral angle H-C-Si-Si, which defines the orientation of the surface methyl groups, was found to be 37.7°, which is in excellent agreement with the value (38°) obtained by Solares *et al.*[31] using the PBE exchange-correlation functional and by Ferguson *et al.*[20] using the Heyd-Scuseria-Ernzerhof (HSE) hybrid functional.

The dynamical matrix was calculated on a 6 × 6 × 1 q-point mesh for the SBZ. In order to improve the readability of the resulting dispersion curves and to highlight the surface modes, the slab thickness was increased up to 30 layers through the insertion of bulk layers. The bulk force constants were obtained on a 6 × 6 × 3 q-point mesh, and then the bulk layers were inserted between the relaxed surface layers. The Fourier transform of the dynamical matrices on a discrete uniform mesh in the SBZ provided the real-space interatomic force constants from which the phonon dispersion relations were calculated. For the calculation of the rotational barrier we employed a 2 × 2 supercell with the same slab configuration used for calculating the dynamical properties but with a 3 × 3 × 1 k-point sampling. In the case of the fully methylated surface we rotated only one methyl while holding the neighboring methyl groups in fixed positions. This approximation provided an upper bound for the rotational barrier since the neighboring methyl groups are not free to rearrange to minimize steric interactions through correlated motion. Calculations involving the isolated methylsilane molecule used a cubic box with a vacuum 15 Å wide and the k-sampling was restricted to the $\bar{\Gamma}$-point.

III. RESULTS AND DISCUSSION

The inelastic helium atom scattering data agreed well with the calculated phonon-dispersion curves, as seen in Figs. 1(d) and 2(d) for CH_3-Si(111) and CD_3-Si(111), respectively. Figures 1 and 2 display representative time-of-flight (TOF) spectra from different regions of the SBZ for both surfaces. These TOF spectra contained elastic features arising

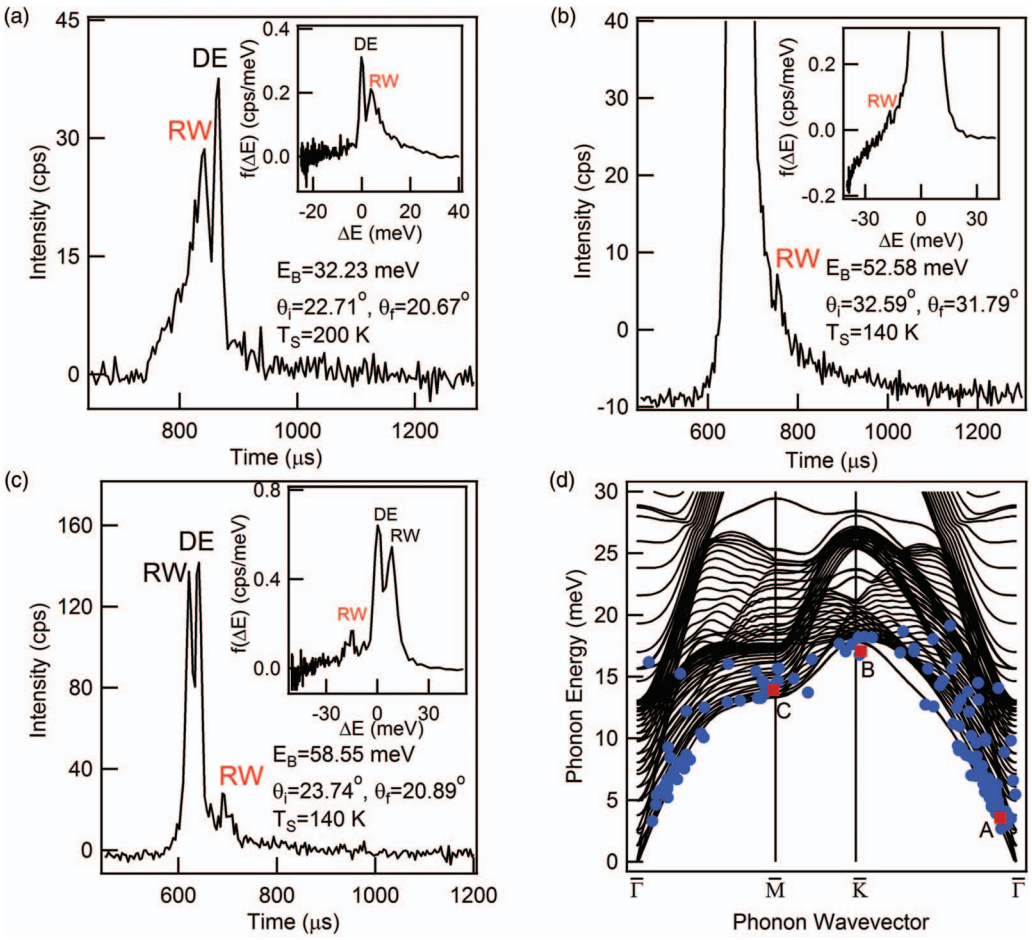

FIG. 1. Representative time-of-flight composite spectra for single phonon inelastic peaks near the $\bar{\Gamma}$-point (a), $\bar{K}$-point (b), and $\bar{M}$-point (c) for the CH_3-Si(111)-(1 × 1) surface. Panel (d) displays the experimental data (blue circles) overlaid on the theoretical dispersion curves, with individual measurements from the three spectra highlighted as red squares.

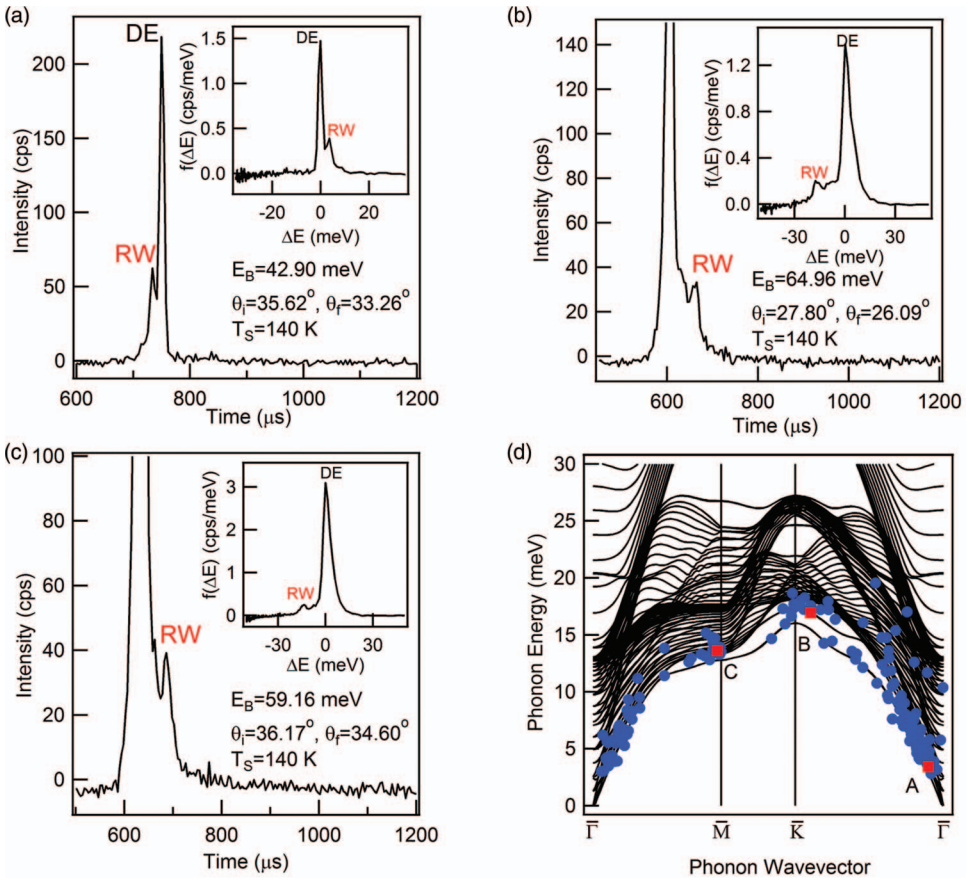

FIG. 2. Representative time-of-flight composite spectra for single phonon inelastic peaks near the $\bar{\Gamma}$-point (a), $\bar{K}$-point (b), and $\bar{M}$-point (c) for the CD_3-Si(111)-(1 × 1) surface. Panel (d) displays the experimental data (blue circles) overlaid on the theoretical dispersion curves, with individual measurements from the three spectra highlighted as red squares.

from the diffuse scattering of atoms due to surface defects and thermal motion, as well as sharp, clear inelastic peaks arising from scattering events in which sufficient momentum is exchanged to create or annihilate a surface vibration. The conservation of energy and crystal momentum defines the observable energy and momentum transfers for a given incident beam energy (E_i), angle of incidence (θ_i), and scattering angle (θ_f). For in-plane scattering, the functional form of these constraints and the resulting scan curve are given in Eqs. (1)–(3):

$$\Delta K = k_f \sin\theta_f - k_i \sin\theta_i = G_{mn} + Q, \tag{1}$$

$$\Delta E = E_f - E_i = \frac{\hbar^2 k_f^2}{2m} - \frac{\hbar^2 k_i^2}{2m} = \pm\hbar\omega(Q), \tag{2}$$

$$\frac{\Delta E}{E_i} = \frac{\left(\sin\theta_i + \Delta K/k_i\right)^2}{\sin^2\theta_f} - 1. \tag{3}$$

In the above equations, G_{mn} is a reciprocal lattice vector, Q is the wavevector for a phonon of energy $\hbar\omega$, m is the mass of the helium atom, k_i is the incident wavevector, and k_f is the scattered, or final, wavevector. By varying the beam energy and the scattering geometry, helium atom scattering provides a survey of the surface phonon dispersions across the entirety of the SBZ.

The low energy regime of the CH_3-Si(111) and CD_3-Si(111) vibrational spectra exhibit a rich and complex behavior characterized by the interplay between three main surface modes: the RW, the methyl rocking mode with respect to the silicon atom, and the hindered rotational mode. Figures 3–5 show the theoretical phonon dispersions for energies up to 70 meV, with the color scale indicating the extent of the contributions to the displacement pattern of a selected atom for a given polarization. The RW dispersion relation for the entire SBZ, obtained from a large number of measurements, agreed well with the theoretical predictions and reveals that the RW hybridizes with the methyl rocking libration near the $\bar{M}$ and $\bar{K}$ points, as described elsewhere.[17] The rocking mode of the methyl with respect to the silicon substrate implies a slight distortion of the internal C-H bonds and the bending of the C-Si bond, and it has an energy of 16 meV at the $\bar{\Gamma}$-point for CH_3-Si(111) and 14 meV for CD_3-Si(111) (see Figs. 3 and 4 panels (e) and (f)). Away from the $\bar{\Gamma}$-point this mode splits into a longitudinal and a shear-horizontal component. For both surfaces, the longitudinal component has an upward dispersion forming the nearly flat surface branch at ∼27.3 meV, while the shear-horizontal component shows a weak downward dispersion. Initially, the shear horizontal mode strongly hybridizes with the bulk modes, then with the RW near the zone edges, which increases the RW energy with respect to the theoretical value obtained by freezing the methyl modes.[17]

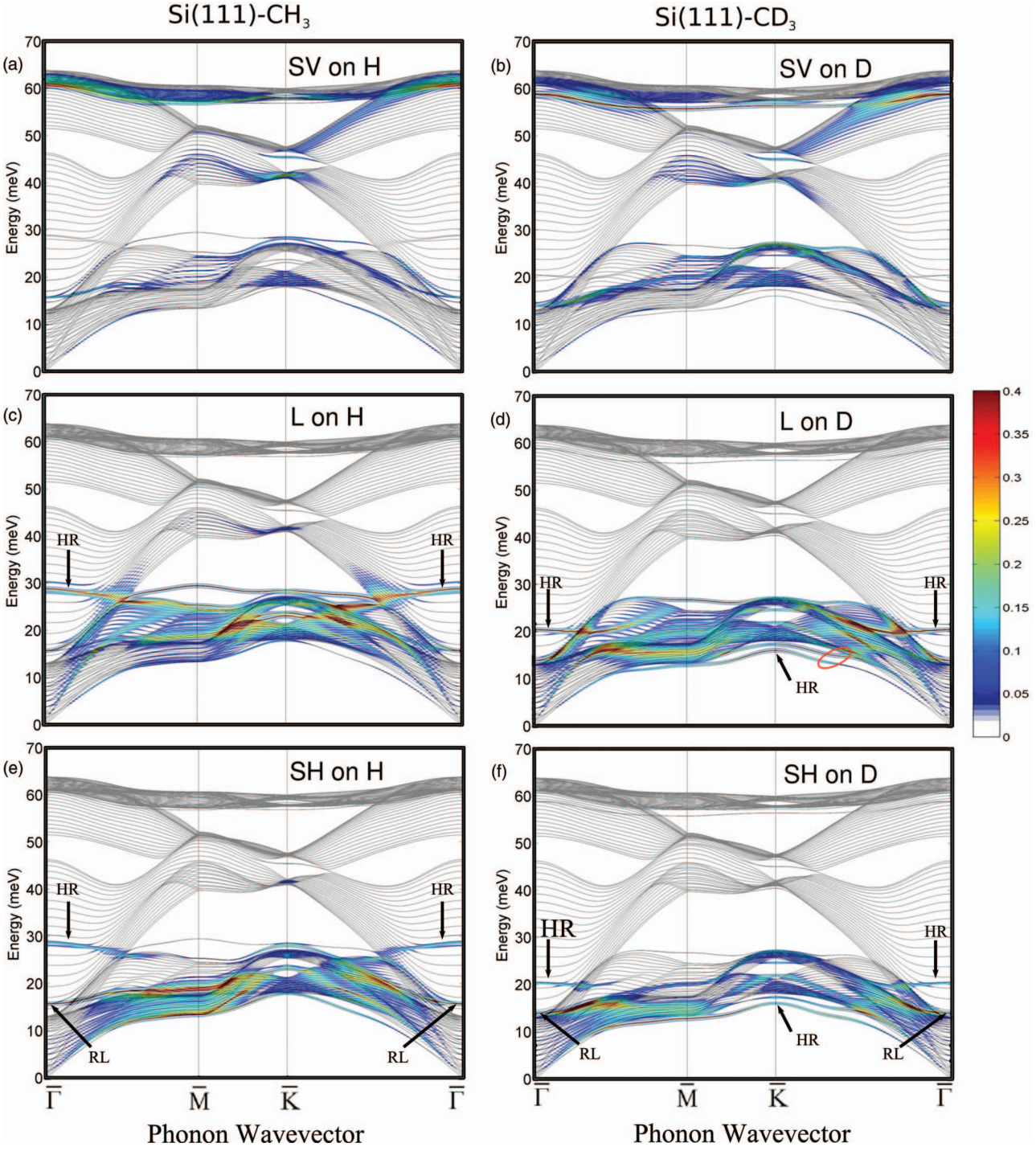

FIG. 3. Theoretical dispersion curves for CH_3-Si(111), left, and CD_3-Si(111), right, for energies up to 70 meV. The color scale indicates the extent of the contributions to the surface displacement pattern from the hydrogen or deuterium atoms for a selected polarization: shear vertical (SV), longitudinal (L), and shear horizontal (SH). The arrows labelled HR indicate the location of the hindered rotation in the SBZ, and the arrows labelled RL indicate the position of the rocking libration. The red circle highlights the region in which the hindered rotation crosses the Rayleigh wave near the $\bar{K}$-point.

In the case of CD_3-Si(111), the RW dispersion is further complicated by the fact that the hindered rotation band intersects the RW at the SBZ boundary, which is noted by the red ellipse in Figs. 3(d) and 4(d). The hindered rotational mode exhibits an energy of 29.0 meV for CH_3-Si(111) and 20.8 meV for CD_3-Si(111) at the $\bar{\Gamma}$-point, and its dispersion is highlighted in Fig. 3 panels (c)-(f.) The ratio of the hindered rotation for the CH_3- and CD_3-terminated surfaces almost exactly reflects the effect of the isotopic substitution, because this libration almost exclusively involves displacements of the hydrogen, or deuterium, atoms. For CH_3-Si(111), the hindered rotation starts merging with the bulk modes midway through the $\overline{\Gamma K}$ direction, then recovers a purely rotational character near the $\bar{K}$-point, and ends in a gap mode of ~23 meV at that zone edge. In the CD_3-Si(111) case, the hindered rotation becomes the lowest-energy mode (16 meV) at the $\bar{K}$-point after

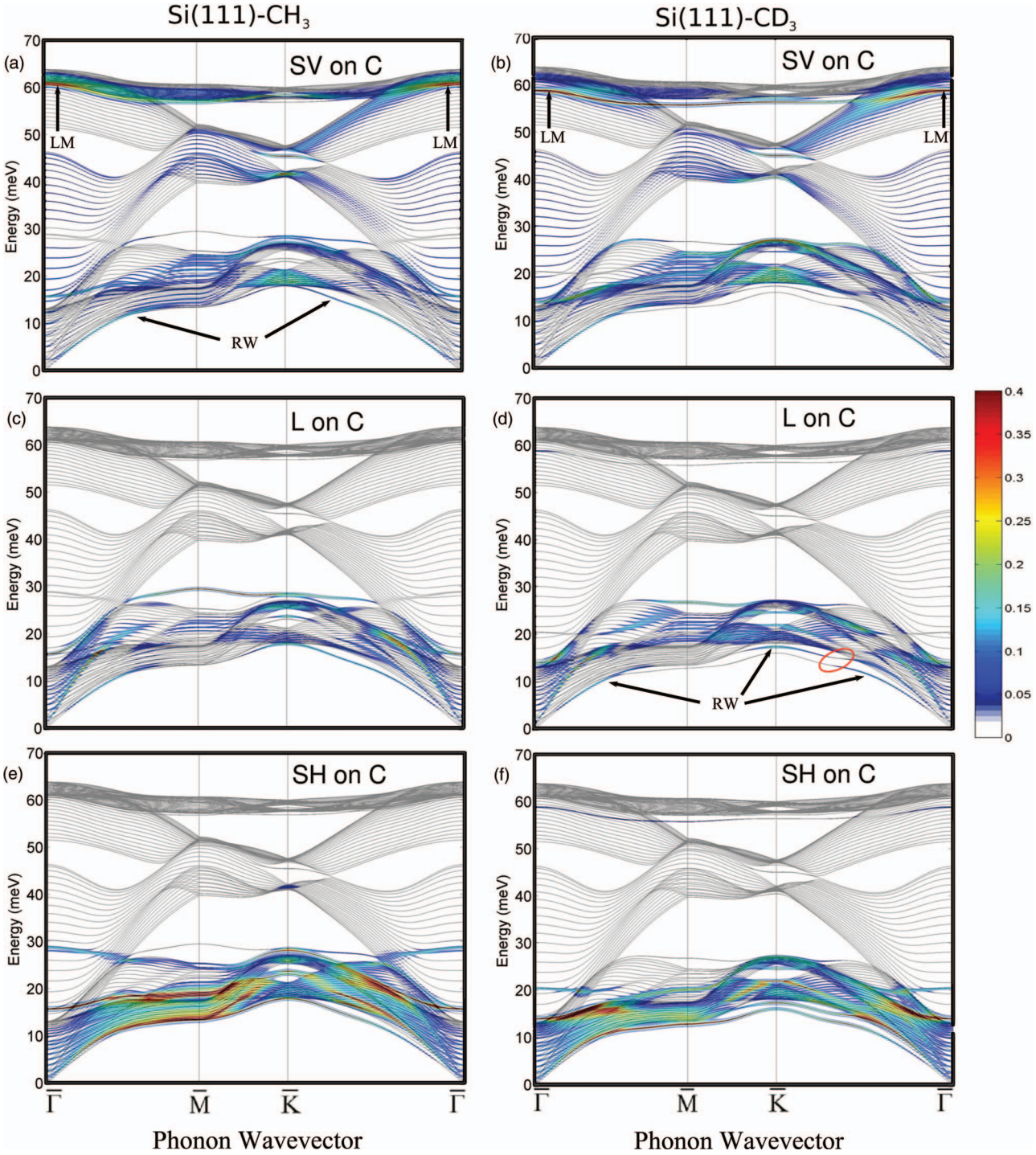

FIG. 4. Theoretical dispersion curves for CH_3-Si(111), left, and CD_3-Si(111), right, for energies up to 70 meV. The color scale indicates the extent of the contributions to the displacement pattern of the carbon atom for a selected polarization: shear vertical (SV), longitudinal (L), and shear horizontal (SH). The arrows labelled RW indicate the Rayleigh wave on the dispersion plot, the arrows labelled LM are the location of the Lucas pair, and the red circle highlights the region in which the hindered rotation crosses the Rayleigh wave.

crossing the Rayleigh wave. The $\bar{\Gamma}$-point hindered rotation energy of 29.0 meV for the CH_3-Si(111) surface is slightly higher than the experimentally observed value of 24.8 meV for the CH_3SiH_3 (methylsilane) molecule,[32] presumably due to the steric interaction between neighboring methyl groups on the surface, which are absent in the gas phase.

The rotational dynamics of the methyl group on the fully methylated silicon surface have recently been investigated experimentally, with the methyl group found to be rotationally hindered at room temperature.[18] To elucidate the role of the substrate and the neighboring methyl groups in preventing this rotation, the activation barrier energy was calculated for the extreme case of a methyl group rotating in a fixed environment on the CH_3-Si(111) surface. This value was compared to the activation barriers of an isolated methyl group on a H-Si(111)-(1 × 1) surface and a single methylsilane molecule

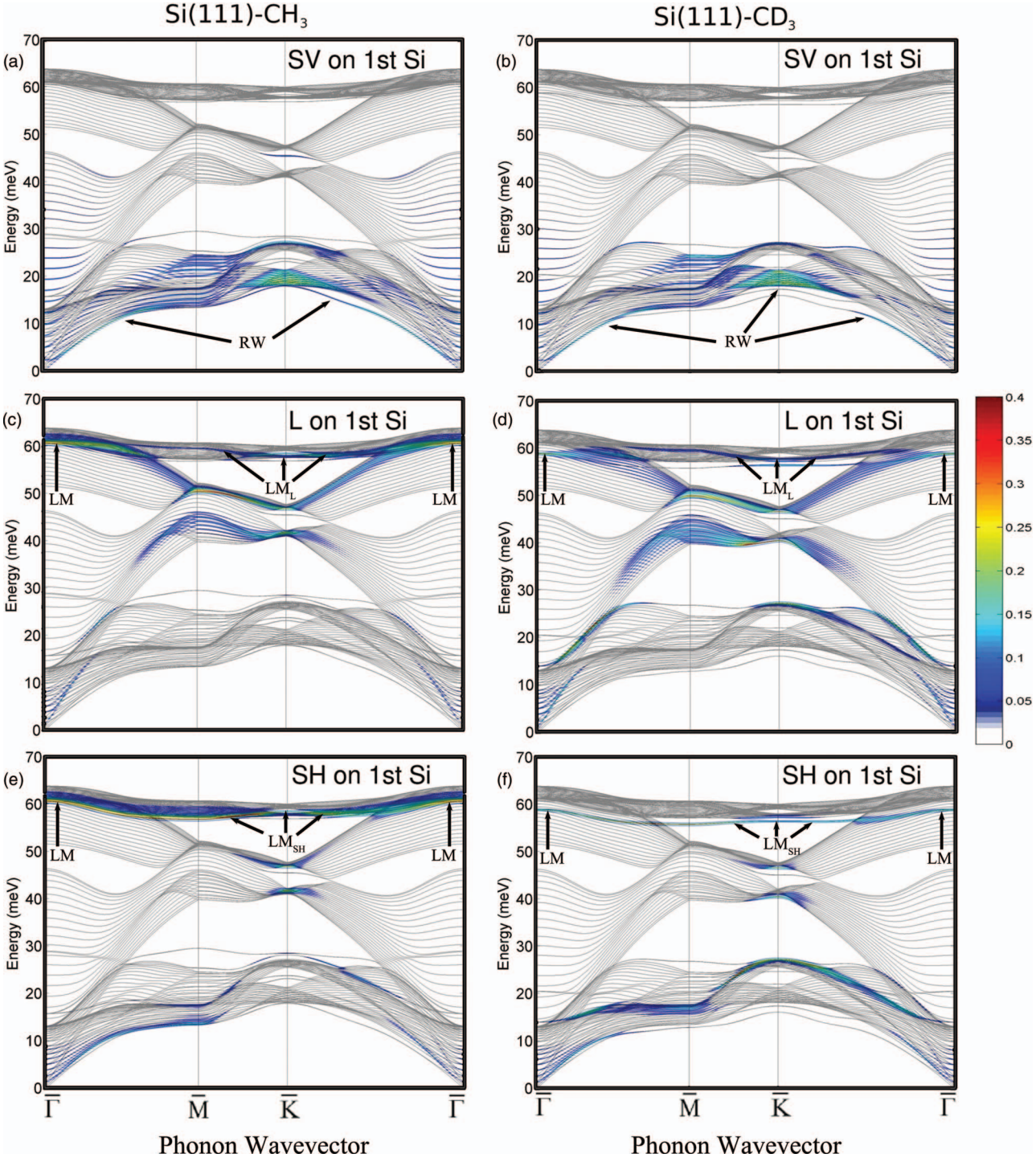

FIG. 5. Theoretical dispersion curves for CH_3-Si(111), left, and CD_3-Si(111), right, for energies up to 70 meV. The color scale indicates the extent of the contributions to the displacement pattern of the most superficial silicon atom for a selected polarization: shear vertical (SV), longitudinal (L), and shear horizontal (SH). The arrows labelled RW indicate the location of the Rayleigh wave, and the arrows labelled LM indicate the position of the Lucas pair. The longitudinal branch of the Lucas pair is indicated by the three arrows labelled LM_L, and the shear-horizontal branch of the Lucas pair is noted with three arrows labelled LM_{SH}.

(Fig. 6). The steric interaction in the fully methylated system considerably increases the activation energy to 112 meV with respect to barriers found for the methylsilane molecule (62 meV in our calculation, 73 meV from experiment[18]) and for the isolated methyl group on a H-Si(111) surface (49.5 meV). In all cases, however, the activation barrier is sufficient to prevent the free rotation of the methyl groups at the CH_3-Si(111) interface. A fourth surface branch was also observed in the low energy range. This mode starts as a broad longitudinal resonance of 4.9 meV near the $\bar{\Gamma}$-point and rises to 14.9 meV near the midpoint of the SBZ, most clearly shown in Fig. 5 panels (c) and (d), then strongly

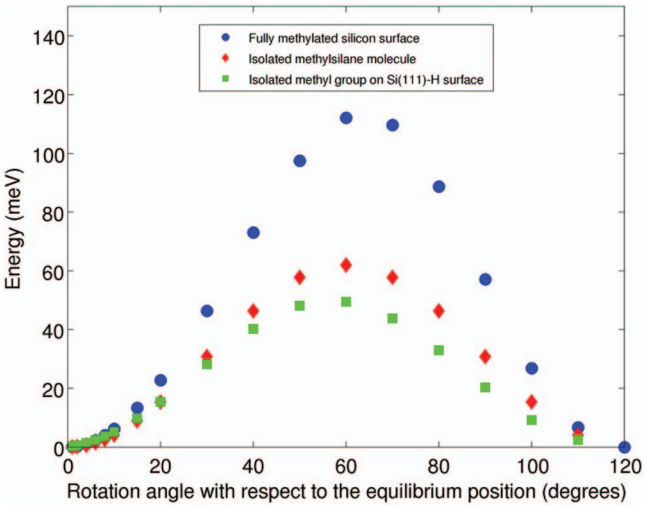

FIG. 6. The change in conformational energy due to the rotation of the methyl-group about the C-Si axis, or surface normal, away from its equilibrium orientation. This energy difference describes the potential which constrains the rotational motion of the methyl group.

hybridizes with the bulk modes before becoming a localized gap mode at the $\bar{K}$-point with an energy of 24.8 meV, as seen at the $\bar{K}$-point in Fig. 4 panels (c) and (d).

Three resonances occur near the $\bar{K}$-point in the intermediate range of the energy spectrum. Two of these resonances appear at 40.9 meV and 49.0 meV, and are associated with the displacements in the first silicon layer (Fig. 5 panels (c)-(f)). The third resonance is a gap mode at the $\bar{K}$-point with an energy of 45.9 meV which arises primarily from the shear-vertical vibration of the C atom (Fig. 4 panels (a) and (b). There is a sharp, nearly dispersionless resonance just below the silicon optical bands with mode energies of 60.8 meV and 58.3 meV at the $\bar{\Gamma}$-point for the CH_3-Si(111) and CD_3-Si(111) surfaces, respectively, which evolves into a pair of surface states as the zone boundary is approached. Although prior work suggested that a mode at 59 meV is associated with a Si-C bending vibration hybridized with surface phonons,[20] the analysis herein indicated that it is an intrinsic Lucas pair, whose evolution through the SBZ is most clearly visualized in Fig. 7, with only a small component arising from the

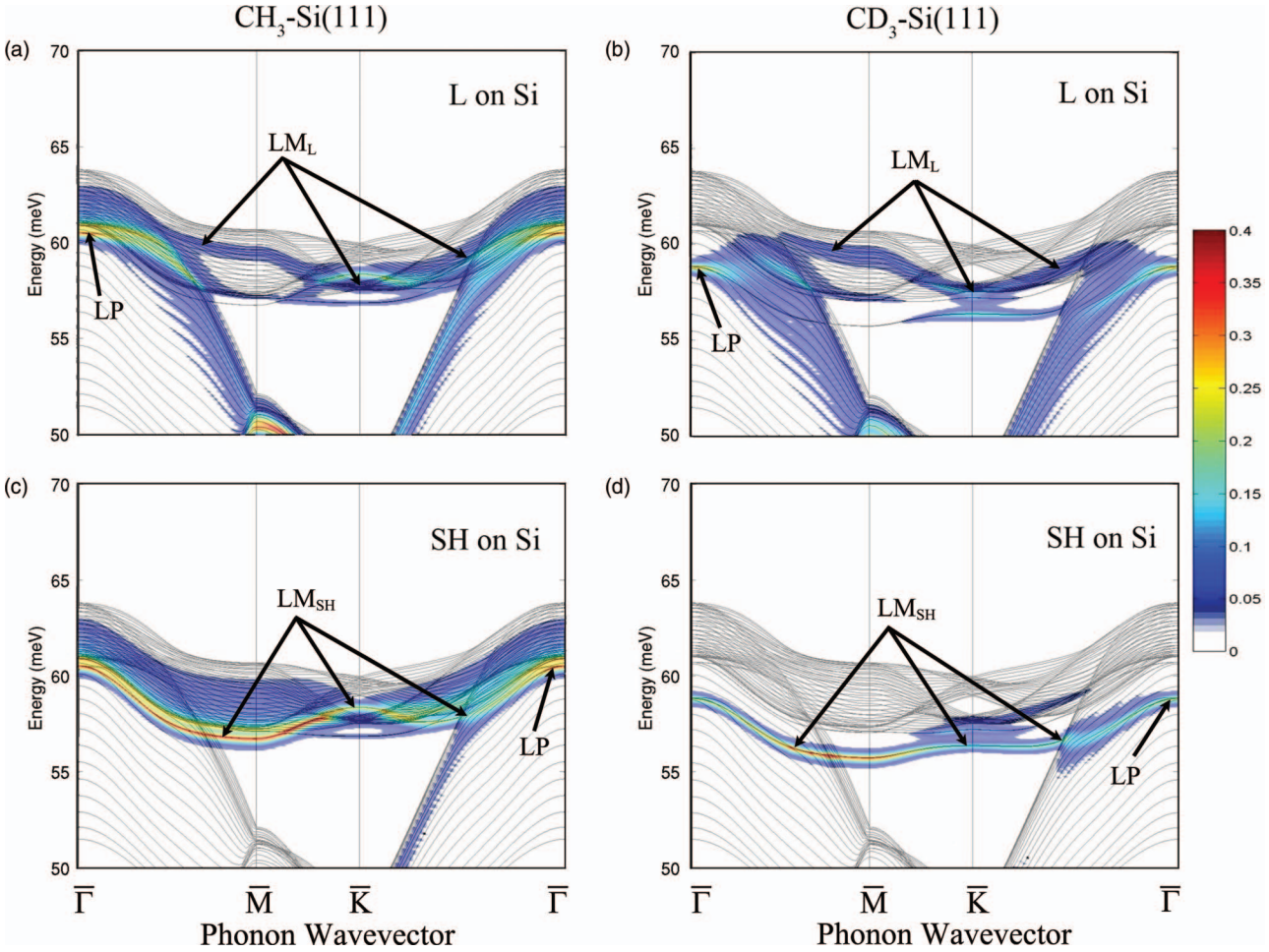

FIG. 7. Theoretical dispersion curves for CH_3-Si(111), left, and CD_3-Si(111), right, for an energy range of 50–70 meV for the longitudinal ((a) and (b)) and shear horizontal ((c) and (d)) polarizations. The color scale indicates the extent of the contributions to the total displacement pattern arising from a given polarization at a specific atom. The arrows labelled LP indicate the position of the Lucas pair near the $\bar{\Gamma}$-point, LM_L is the longitudinal branch of the Lucas pair, and LM_{SH} is the shear-horizontal branch of the Lucas pair.

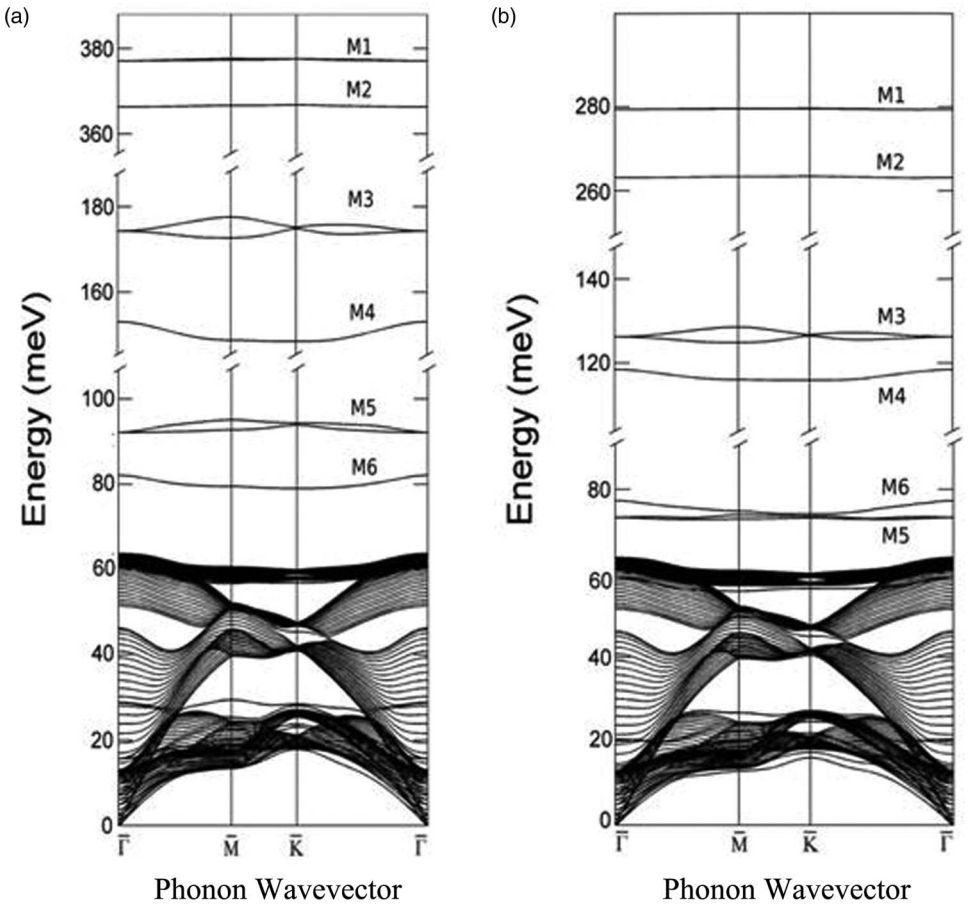

FIG. 8. Theoretical dispersion curves for CH_3-Si(111) (a), and CD_3-Si(111) (b), for the entire vibrational energy spectrum.

shear-vertical vibration of the carbon atom (Fig. 4 panels (a) and (b). Lucas modes, originally discovered in the surfaces of cubic ionic crystals, constitute a pair of microscopic optical surface phonons which have in-plane polarization and are degenerate at the $\bar{\Gamma}$-point for hexagonal or square surface symmetry.[33] These modes have been predicted and observed for the H-Si(111)-(1 × 1) surface with an energy at the $\bar{\Gamma}$-point ranging from 58.7 to 62 meV.[34–36] The results of our calculations indicated that for the methylated Si(111) surface, the Lucas pair is degenerate at the $\bar{\Gamma}$-point, as required by symmetry, and then splits as it evolves toward the SBZ edges. The longitudinal component hybridizes with the continuum of longitudinal bulk modes, transforming into a broad resonance, while the shear horizontal mode partially hybridizes with the shear vertical vibrations of the carbon atom and maintains a well-defined surface character throughout the SBZ.

The high-energy portion of the spectrum is dominated by the modes involving the deformation of the methyl group. These modes were previously calculated for CH_3-Si(111) at the $\bar{\Gamma}$-point both using a cluster model and PBC[20] and have been studied experimentally by means of HREELS[37] and surface infrared spectroscopy.[13–15] Figure 8 shows the dispersion of these modes for both the CH_3-Si(111) and CD_3-Si(111) surfaces. Table I summarizes the predicted methyl-vibrational

TABLE I. CH_3-Si(111) methyl vibrational energies at the $\bar{\Gamma}$-point (meV).

Mode[a]	PBE+PW	Cluster[b]	PBC-6[b]	HREELS[c]	IR[d,e,f]
M1 (CH_3 asymmetric stretch)	377.2	379.8	379.7	365.0	367.9[d], 367.7[e], 367.0[f]
M2 (CH_3 symmetric stretch)	366.4	370.8	371.2	...	353.9[d], 360.7[e], 359.6[f]
M3 (CH_3 asymmetric deformation)	174.3	178.9	179.2	176.4	174.9[f]
M4 (CH_3 symmetric deformation)	153.1	158.0	158.4	157.2	156.0[d], 155.8[e], 155.6[f]
M5 (CH_3 internal rocking)	92.1	97.0	94.7	97.8	93.5[d], 93.9[e]
M6 (C-Si stretch)	82.1	79.0	79.7	84.7	84.1[d]

[a]Modes labelled using the same convention as Fig. 8.
[b]Reference 20.
[c]Reference 37.
[d]Reference 13.
[e]Reference 14.
[f]Reference 15.

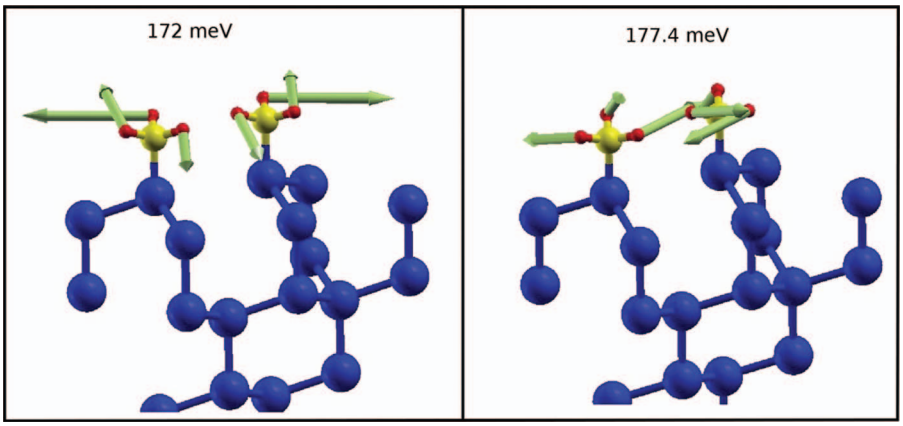

FIG. 9. Eigenvectors corresponding to the two asymmetric deformations at the $\bar{M}$-point. The displacement pattern of the high-energy mode brings the hydrogen atoms into closer proximity to each other than the displacement pattern of the low energy mode. The splitting of the asymmetric deformation orginates from the resulting difference in steric interactions. The magnitude of the eigenvectors has been enhanced for clarity.

energies for the CH_3-Si(111) surface and presents a comparison with results from previous calculations and experimental data on this system. Across the SBZ, both the symmetric and asymmetric stretching modes show a nearly dispersionless character with a bandwidth of only 0.25 meV. In contrast, the asymmetric deformation away from the $\bar{\Gamma}$-point splits into two components which reach a maximum separation at the $\bar{M}$-point, with the upper branch at 177.4 meV and the lower branch at 172.5 meV. Since the substrate remained unchanged within the frozen substrate approximation, the splitting is attributed to the different interactions between neighboring methyl groups. Figure 9 presents a schematic of the asymmetric deformation eigenvectors at the $\bar{M}$-point, with the difference in the eigendisplacements of the high and low energy branches showing a clear disparity in the proximity of the hydrogen atoms of adjacent methyl groups, which leads to the mode splitting. A similar behavior was predicted for the internal rocking vibrational mode, which exhibits a splitting of 2.5 meV at the $\bar{M}$-point. The C-Si stretch exhibits a bandwidth of 4.4 meV with a minimum near the $\bar{K}$-point, which mainly is due to contributions from the shear-vertical displacements of the first layer silicon atom.

As provided by the DFPT calculations, Table II summarizes the effects of the isotopic substitution of H with D on these high energy modes. Except for the C-Si stretching mode, the vibrational energies of CD_3-Si(111) are related to those of CH_3-Si(111) according to the square root of the mass ratio, $(m_H/m_D)^{1/2}$. The systematically higher values of the calculated energies with respect to the mass ratio rule reflect the (small) contribution of the carbon atom displacements, which remain unchanged in CH_3-Si(111) and CD_3-Si(111). The isotopic effect on the C-Si stretch is consistent with this mode involving the motion of the methyl group as a whole and, therefore, corresponds to the mass ratio rule for the entire CH_3 and CD_3 groups, which is a substantially smaller effect than that observed in modes mainly involving the displacements of the H or D atoms.

TABLE II. Vibrational energies (meV) at the $\bar{\Gamma}$-point obtained from the PBE+PW calculations.

Mode	CH_3-Si(111)	CD_3-Si(111)
M1 (asymmetric stretch)	377.2	279.2
M2 (symmetric stretch)	366.4	262.8
M3 (asymmetric deformation)	174.3	126.1
M4 (symmetric deformation)	153.1	118.4
M5 (internal rocking)	92.1	73.2
M6 (C-Si stretch)	82.1	77.2

IV. CONCLUSIONS

The present study of the methyl-terminated silicon (111) surface with helium atom scattering and density functional perturbation theory has clearly characterized the effects of organic functionalization on the surface vibrations of a hybrid organic-semiconductor interface. The helium atom scattering experiments elucidated the Rayleigh wave dispersion relation across the entire surface Brillouin zone, and, with the aid of DFPT calculations, provided insight into the interaction of the Rayleigh wave with the low-energy rocking libration and hindered rotation of the methyl group. The theoretical calculations predicted a rotational barrier height that inhibits the free rotation of the methyl group about the C-Si axis at room temperature, which is in agreement with a recent sum frequency generation study of this surface.[18] This theoretical work also provided a comprehensive discussion of the other surface phonon modes and resonances for the methyl-terminated surface. Specifically, Lucas modes have been identified for both the CH_3-Si(111) and CD_3-Si(111) surfaces, which split into their longitudinal and shear-horizontal components as the pair evolves across the SBZ. Analysis of the deformations for both the CH_3- and CD_3-terminal groups showed that several modes exhibit splitting as a result of steric interactions between neighboring methyl groups. The CH_3-Si(111) deformations are in agreement with the values previously reported in the literature, and the shifts in CD_3-Si(111) vibrational energies are consistent with the expected impact of isotopic substitution. This combined theoretical and experimental effort clearly demonstrates the impact of organic functionalization on the surface phonons of a semiconductor lattice. Specifically, both the hybridization of molecular

librations with lattice phonons and the steric interactions between adjacent organic terminal groups play a significant role in defining the surface vibrational band structure of hybrid organic-semiconductor interfaces.

ACKNOWLEDGMENTS

S.J.S. acknowledges support from the Air Force Office of Scientific Research (AFOSR) Grant No. FA9550-10-1-0219, and the Material Research Science and Engineering Center at the University of Chicago for infrastructure support, and N.S.L. acknowledges support from the National Science Foundation (NSF) (CHE-1214152).

[1]H. N. Waltenburg and J. T. Yates, Chem. Rev. **95**, 1589 (1995).
[2]J. M. Buriak, Chem. Rev. **102**, 1271 (2002).
[3]P. Thissen, O. Seitz, and Y. J. Chabal, Prog. Surf. Sci. **87**, 272 (2012).
[4]M. Y. Bashouti, K. Sardashti, S. W. Schmitt, M. Pietsch, J. Ristein, H. Haick, and S. H. Christiansen, Prog. Surf. Sci. **88**, 39 (2013).
[5]H. Haick, P. T. Hurley, A. I. Hochbaum, P. Yang, and N. S. Lewis, J. Am. Chem. Soc. **128**, 8990 (2006).
[6]A. Bansal and N. S. Lewis, J. Phys. Chem. B **102**, 4058 (1998).
[7]T. Osaka, M. Matsunaga, S. Kudo, D. Niwa, Y. Shacham-Diamand, W. Jaegermann, and R. Hunger, J. Electrochem. Soc. **154**, H919 (2007).
[8]X. Shen, B. Sun, F. Yan, J. Zhao, F. Zhang, S. Wang, X. Zhu, and S. Lee, ACS Nano **4**, 5869 (2010).
[9]T. L. Lasseter, B. H. Clare, N. L. Abbott, and R. J. Hamers, J. Am. Chem. Soc. **126**, 10220 (2004).
[10]W. Yang and R. J. Hamers, Appl. Phys. Lett. **85**, 3626 (2004).
[11]L. J. Webb and N. S. Lewis, J. Phys. Chem. B **107**, 5404 (2003).
[12]W. J. Royea, A. Juang, and N. S. Lewis, Appl. Phys. Lett. **77**, 1988 (2000).
[13]S. Rivillon and Y. J. Chabal, J. Phys. IV **132**, 195 (2006).
[14]L. J. Webb, S. Rivillon, D. J. Michalak, Y. J. Chabal, and N. S. Lewis, J. Phys. Chem. B **110**, 7349 (2006).
[15]A. Fidélis, F. Ozanam, and J.-N. Chazalviel, Surf. Sci. **444**, L7 (2000).
[16]J. S. Becker, R. D. Brown, E. Johansson, N. S. Lewis, and S. J. Sibener, J. Chem. Phys. **133**, 104705 (2010).
[17]R. D. Brown, Z. M. Hund, D. Campi, L. E. O'Leary, N. S. Lewis, M. Bernasconi, G. Benedek, and S. J. Sibener, Phys. Rev. Lett. **110**, 156102 (2013).
[18]S. Malyk, F. Y. Shalhout, L. E. O'Leary, N. S. Lewis, and A. V. Benderskii, J. Phys. Chem. C **117**, 935 (2013).
[19]R. D. Brown, Q. Tong, J. S. Becker, M. A. Freedman, N. A. Yufa, and S. J. Sibener, Faraday Discuss. **157**, 307 (2012).
[20]G. A. Ferguson and K. Raghavachari, J. Chem. Phys. **125**, 154708 (2006).
[21]H. Kato, T. Taoka, S. Suto, T. Motoya, A. Kasuya, and T. Yamada, Phys. Rev. B **75**, 085319 (2007).
[22]B. Sandfort, A. Mazur, and J. Pollmann, Phys. Rev. B **51**, 7139 (1995).
[23]V. Graschus, A. Mazur, and J. Pollmann, Surf. Sci. **368**, 179 (1996).
[24]G. Benedek, M. Bernasconi, K.-P. Bohnen, D. Campi, E. V. Chulkov, P. M. Echenique, R. Heid, I. Y. Sklyadneva, and J. P. Toennies, Phys. Chem. Chem. Phys. **16**, 7159 (2014).
[25]A. Bansal, X. Li, I. Lauermann, N. S. Lewis, S. I. Yi, and W. H. Weinberg, J. Am. Chem. Soc. **118**, 7225 (1996).
[26]B. Gans, P. A. Knipp, D. D. Koleske, and S. J. Sibener, Surf. Sci. **264**, 81 (1992).
[27]P. Giannozzi *et. al.*, J. Phys. Condens. Matter **21**, 395502 (2009).
[28]D. Vanderbilt, Phys. Rev. B **41**, 7892 (1990).
[29]J. P. Perdew, K. Burke, and M. Ernzerhof, Phys. Rev. Lett. **77**, 3865 (1996).
[30]H. J. Monkhorst and J. D. Pack, Phys. Rev. B **13**, 5188 (1976).
[31]S. D. Solares, H. Yu, L. J. Webb, N. S. Lewis, J. R. Heath, and W. A. Goddard, J. Am. Chem. Soc. **128**, 3850 (2006).
[32]G. Pelz, P. Mittler, K. M. T. Yamada, and G. Winnewisser, J. Mol. Spectrosc. **156**, 390 (1992).
[33]A. A. Lucas, J. Chem. Phys. **48**, 3156 (1968).
[34]U. Harten, J. Toennies, C. Wöll, L. Miglio, P. Ruggerone, L. Colombo, and G. Benedek, Phys. Rev. B **38**, 3305 (1988).
[35]R. Honke, P. Pavone, and U. Schröder, Surf. Sci. **367**, 75 (1996).
[36]R. Honke, P. Jakob, Y. J. Chabal, A. Dvořák, S. Tausendpfund, W. Stigler, P. Pavone, A. P. Mayer, and U. Schröder, Phys. Rev. B **59**, 10996 (1999).
[37]T. Yamada, M. Kawai, A. Wawro, S. Suto, and A. Kasuya, J. Chem. Phys. **121**, 10660 (2004).